THE ASTROPHYSICAL JOURNAL, 534:670–683, 2000 May 10

RADIAL DISTRIBUTION OF THE MASS-TO-LUMINOSITY RATIO IN SPIRAL GALAXIES AND MASSIVE DARK CORES

TSUTOMU TAKAMIYA AND YOSHIAKI SOFUE
Institute of Astronomy, University of Tokyo, Mitaka, Tokyo 181-8588, Japan
Received 1999 May 19; accepted 1999 November 24

ABSTRACT

We derive radial profiles of the surface mass density for 19 spiral galaxies directly from their high-resolution rotation curves. Using the corresponding luminosity profiles, we obtain the radial distribution of the mass-to-luminosity ratios (M/Ls) from the inner bulge (around a few hundred parsecs) to the outer disk ($\geq$2–10 kpc) for 11 galaxies (with inclination $<70^\circ$ in order to reduce the influence of the interstellar extinction). The M/Ls in the bulges of two galaxies with sufficient resolution, NGC 4527 and NGC 6946, are found to increase steeply toward the center at radii $\sim$100–500 pc at rates of 15 ± 3 and 7 ± 2 times per kpc, respectively. Some other galaxies with fairly high resolution also show signs of an increase toward the center. Such an increase may indicate the existence of a new component, a "massive dark core," which may be an object linking the bulge and a central black hole. Based on radial variations of the M/Ls, we further discuss the variation of the dark mass fraction in spiral galaxies.

Subject headings: galaxies: kinematics and dynamics — galaxies: photometry — galaxies: spiral — galaxies: structure

1. INTRODUCTION

A radial variation of the mass-to-luminosity ratio (M/L) in a galaxy is a clue to investigate the distribution of visible and dark (invisible) masses (e.g., Kent 1986, 1987; Persic & Salucci 1988, 1990; Salucci & Frenk 1989; Forbes 1992; Persic, Salucci, & Stel 1996; Héraudeau & Simien 1997; Rubin, Kenny, & Young 1997). However, most of the current studies have been devoted to investigating the dark halo, which is supposed to be closely related to galaxy formation and the stability of disks (e.g., Ostriker & Peebles 1973; Athanassoula, Bosma, & Papaioannou 1987). On the other hand, there have been few systematic investigations of dark matter within a bulge or an inner disk, for which, however, high-resolution and high-quality rotation curves as well as corresponding luminosity profiles are required.

Rotation curves (RCs) in disk and outer regions have been derived from position-velocity diagrams obtained by optical and H I line spectroscopy (Rubin, Ford, & Thonnard 1980, 1982; Rubin et al. 1985; Bosma 1981a; Mathewson, Ford, & Buchhorn 1992; Persic & Salucci 1995; Mathewson & Ford 1996; Clemens 1985; Sofue 1996, 1997; Honma & Sofue 1997a, 1997b). Recently, we have obtained innermost RCs by analyzing high-resolution CO, Hα, and [N II] line spectroscopic data (Sofue 1996, 1997; Sofue et al. 1997, 1998, 1999). Figure 1 shows RCs of Sb and Sc galaxies (e.g., Sofue 1997) thus obtained. All the Sb galaxies in our sample show very steep increases in rotation velocity in the central 100–500 pc region. The Sc galaxies also show similar nuclear increases, except for a few small-mass galaxies, which show rigid-body growth in the RCs. Figure 1 includes some barred galaxies, which also show similar rotation properties to those of normal galaxies. Recent CCD observations of the Hα line have also revealed the nuclear increases in rotation velocity for many galaxies (Rubin et al. 1997; Sofue et al. 1997, 1998, 1999; Bertola et al. 1998), in agreement with the CO results. It is also interesting to note that the rotation velocities in many galaxies do not appear to decline to zero at the nuclei, indicating that the mass density increases steeply toward the center (Bertola et al. 1998; Sofue et al. 1999).

The fact that almost all the galaxies show steep nuclear increases would imply that the high velocities are not due to noncircular motions in bars. When a bar is observed, the probability of looking it at from a side-on view is significantly higher than that from an end-on view. If the influence of noncircular motion is significant, the RC will indicate lower and more gradually rising velocity than the circular velocity, rather close to the pattern speed of the bar. Therefore, we may assume that the RCs trace the circular motions in the first approximation. If bars exist, we may still underestimate the circular velocity, which would result in an underestimated mass density.

Radial profiles of the surface mass density (SMD) and the surface luminosity can be used to calculate the M/L directly. As for SMD profiles, Bosma (1981b) used two methods, described by Nordsieck (1973) and Shu, Stachnik, & Yost (1971), to derive them directly from RCs. He compared these methods and found a good agreement between the two SMD profiles. However, most of the current investigations have been done on the assumption that the visible part of a galaxy consists of a given set of a bulge and a disk, each assumed to have a constant M/L. Although this idea is useful for quantifying the averaged characteristics in each component, it is necessary to confirm whether the assumption of a constant M/L is reliable. Kent (1986) has extensively used the "maximum-disk method" to fit RCs calculated on this assumption to observed RCs: he has derived averaged M/Ls in the individual components. However, this method is based on the assumption that there is no dark matter in the bulge and disk. Moreover, results of such a fitting process depend heavily on bumps and wiggles in the luminosity profiles (Bosma 1998) as well as on the fitting range.

Forbes (1992) has derived the radial variation of the ratio of the total mass to total luminosity involved within a radius r, which can be called an "integrated M/L." In this paper, we will derive both the SMD and the surface luminosity as differential quantities at a given radius and compare them directly in order to discuss the detailed radial distribution of the M/L.

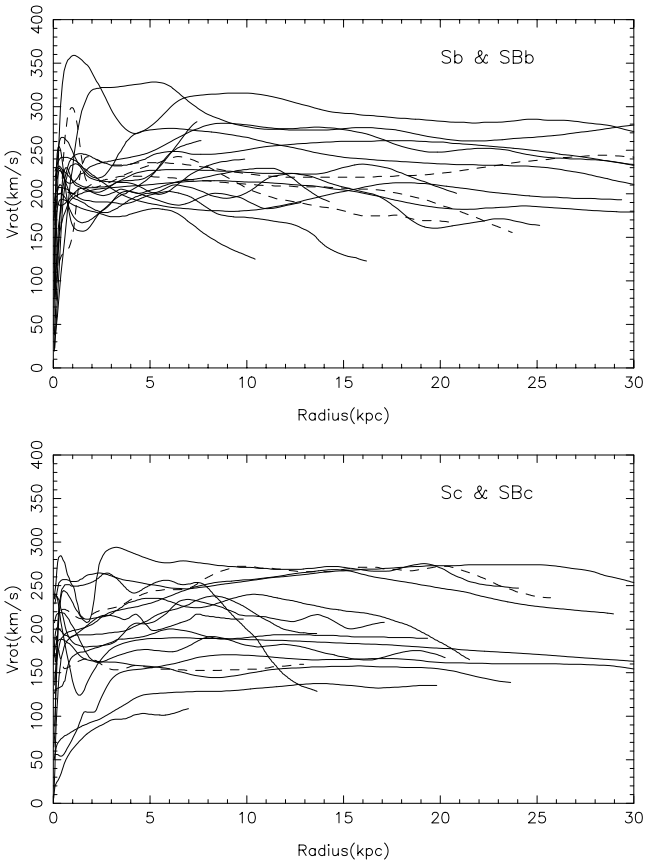

FIG. 1.—*Top:* Rotation curves of 15 Sb (*solid lines*) and three SBc (*dashed lines*) galaxies. *Bottom:* Rotation curves of 15 Sc (*solid lines*) and two SBc (*dashed lines*) galaxies. Note that small-mass galaxies, whose maximum disk velocities are 100–200 km s^{-1}, tend to show mild increases.

In § 2, we derive the SMD profiles. We obtain the luminosity profiles in § 3, describe the obtained M/L profiles in § 4, and discuss the results in § 5.

2. RADIAL PROFILES OF THE SURFACE MASS DENSITY

We assume that the "true" mass distribution in a real disk galaxy will be between two extreme cases, spherical and axisymmetric flat-disk distributions. We can calculate the SMD, $\sigma(R)$, directly from an RC for these extreme cases.

2.1. *Spherical Mass Distribution*

The mass $M(r)$ inside the radius r is given by

$$M(r) = \frac{rV(r)^2}{G}, \tag{1}$$

where $V(r)$ is the rotation velocity at r. Then the SMD $\sigma_S(R)$ at R is calculated by

$$\sigma_S(R) = 2\int_0^\infty \rho(r)\,dz \tag{2}$$

$$= \frac{1}{2\pi}\int_R^\infty \frac{1}{r\sqrt{r^2 - R^2}}\frac{dM(r)}{dr}\,dr\,. \tag{3}$$

Here, R, r, and z are related by $r = (R^2 + z^2)^{1/2}$ and the volume mass density $\rho(r)$ is given by

$$\rho(r) = \frac{1}{4\pi r^2}\frac{dM(r)}{dr}\,. \tag{4}$$

For a given RC, $V(r)$, equation (3) can be calculated numerically. Note, nevertheless, an underestimation of equation (3) becomes significant when $R \sim R_{\max}$, the outermost measured radius of the RC, because equation (3) can be integrated only up to $R_{\max}$ instead of to infinity. This edge effect is negligible elsewhere because of the factor $(r^2 - R^2)^{-1/2}$, by which the contribution at r far from R decreases rapidly. In Figure 2 we show several results of the integration in equation (3) for the Miyamoto-Nagai potential (Miyamoto & Nagai 1975) by taking several different values of $R_{\max}$. Here, the "true" value for this potential is given by $\sigma_D(R)$. The figure demonstrates that the edge effect is almost negligible except at radii $r > 0.9R_{\max}$, where the SMD is underestimated.

2.2. *Flat-Disk Mass Distribution*

The SMD for a thin flat disk, $\sigma_D(R)$, is derived by solving the Poisson equation:

$$\sigma_D(R) = \frac{1}{\pi^2 G}\left[\frac{1}{R}\int_0^R \left(\frac{dV^2}{dr}\right)_x K\left(\frac{x}{R}\right)dx + \int_R^\infty \left(\frac{dV^2}{dr}\right)_x K\left(\frac{R}{x}\right)\frac{dx}{x}\right], \tag{5}$$

where K is the complete elliptic integral and becomes very large when $x \simeq R$ (Binney & Tremaine 1987).

When we calculate the $\sigma_D(R)$, the following three points must be taken into account. First, equation (5) is subject to the boundary condition, $V(0) = V(\infty) = 0$. The assumption $V(0) = 0$ may not be applied if there is a black hole (BH) at the galactic center. However, a central BH with mass of several to hundreds of millions of solar masses dominates the RC only within a few parsecs, and it does not influence the SMD except at the center. On the other hand, the spatial resolution in our data is of the order of 100 pc; thus, the RCs could hardly trace the central BH. Thus, for our purposes we can safely ignore its existence. Second, when calculating the first term on the right-hand side of equation (5), we have only a few data points in the central region

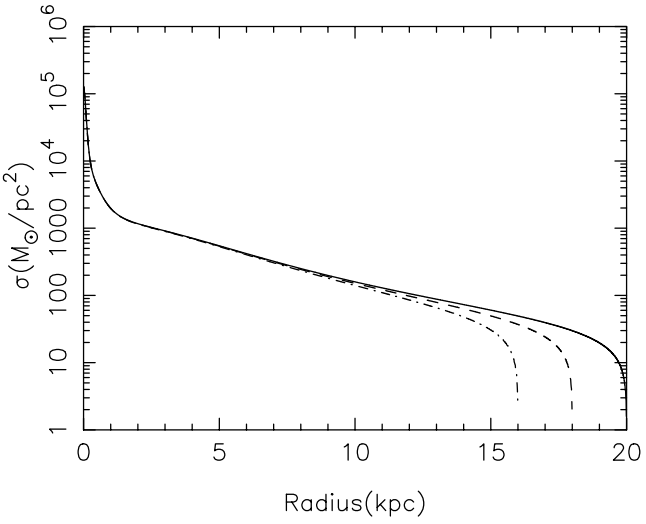

FIG. 2.—Surface mass density profiles calculated from a rotation curve given by the Miyamoto-Nagai potential of our Galaxy under an assumption of spherical mass distribution. Results for different maximum radii, $R_{\max} = 20$ (*solid line*), 18 (*dashed line*), and 16 (*dot-dashed line*) kpc for the upper limit of the integral in eq. (3) in place of infinity are shown.

within a radius comparable to the spatial resolution, where the reliability of the calculated $V(r)$ is lower than in the outer region. Third, the upper limit of the integration of the second term is $R_{\max}$ instead of infinity. Since the RCs are nearly flat or declining outward from $R = R_{\max}$, the second term becomes negative. Hence, we overestimate $\sigma_D(R)$ at $R \simeq R_{\max}$, and, as calculated here, the SMD near the outer edges will give an upper limit to the true value. For such galaxies as NGC 1068 and NGC 4569, whose rotation velocities appear to increase even outward of $R = R_{\max}$, the error would be still larger.

2.3. *Verification Using the Miyamoto-Nagai Potential*

We here examine how the results for the spherical and flat-disk assumptions differ from each other as well as from the "true" SMD by adopting the Miyamoto-Nagai (MN) potential (Miyamoto & Nagai 1975), which realistically comprises four components denoting a compact nucleus, a bulge, a disk, and a dark halo. Given a set of parameters for the MN potential suitable for our Galaxy, we can calculate the true SMD as well as the RC. Using this RC, we derive the SMD for both the spherical and flat-disk assumptions using the same methods as in the previous sections. The MN potential is given by $\Phi = \sum_{i=1}^{4} GM_i\{r^2 + [a_i + (z^2 + b_i^2)^{0.5}]^2\}^{-0.5}$ and $(a_{1-4}, b_{1-4}, M_{1-4}) = (0.00, 0.12, 0.05)$, $(0.00, 0.75, 0.10)$, $(6.00, 0.50, 1.60)$, $(15.00, 15.00, 3.00)$ in units of (kpc, kpc, $10^{11}\ M_\odot$).

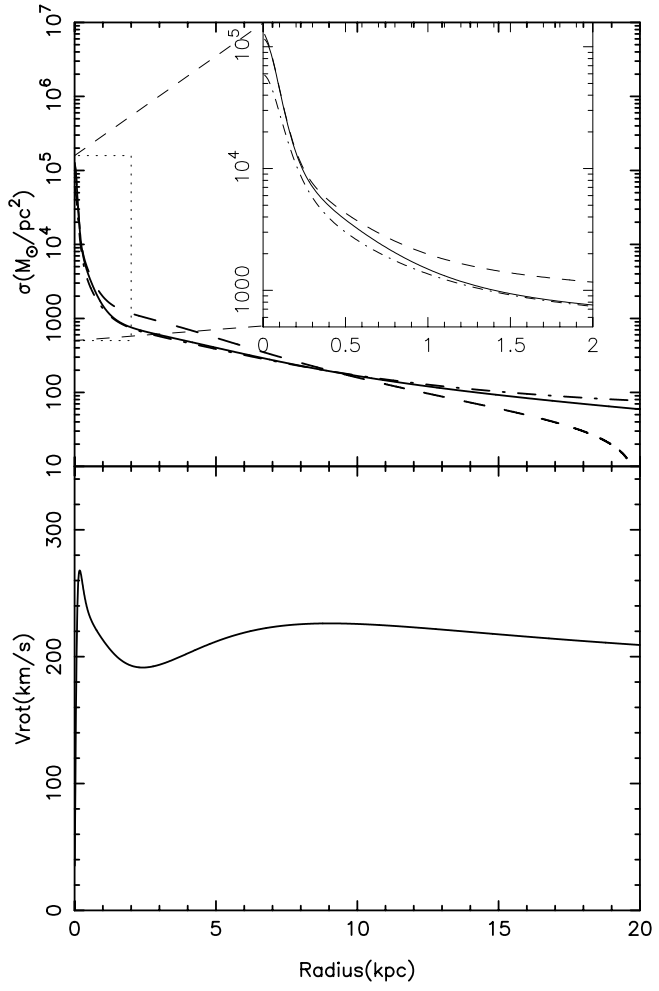

FIG. 3.—*Top:* Real SMD (*solid line*), spherical (*dashed line*), and flat-disk (*dot-dashed line*) SMD profiles calculated for the rotation curve of the Miyamoto-Nagai potential. The upper limit of the integration is taken as $R_{\max} = 20$ kpc in place of infinity. *Bottom:* Rotation curve by the Miyamoto-Nagai model of our Galaxy.

In Figure 3 we show the calculated true SMD and the SMDs for the spherical and flat-disk assumptions calculated from the RC. We used the RC only up to $R = 20$ kpc. Figure 3 shows that the spherical case reproduces well the true SMD for the inner region. This is not surprising because a spherical component is dominant within the bulge. On the other hand, the flat-disk case mimics the true one in the disk region, which is also reasonable. Near the outer edge, the flat-disk case also appears to be a better tracer of the true SMD. We stress that the results from the two extreme assumptions, spherical and flat-disk, differ at most by a factor of 2 and do not differ by more than a factor of 1.5 from the true SMD. We may thus safely assume that the true SMD is in between the two extreme cases: it is better represented by a spherical model for the inner region, while a flat-disk model is better for the disk and outer part.

2.4. *The Data and Results*

We use the RCs in Sofue (1997) to derive the SMD profiles. We select 18 Sa and SAb spiral galaxies for which the spatial resolution (FWHM) is less than 650 pc. Figure 4 shows the calculated $\sigma_S(R)$ and $\sigma_D(R)$ with error bars, respectively. Among the sample, NGC 4527 has the highest signal-to-noise ratio, which has been obtained from CO, H I, and Hα line data. The parameters of the sample are listed in Table 1.

From Figure 4 the typical difference of SMD values between the two assumptions (sphere and flat-disk) is estimated to be ± 0.05–0.1 on a logarithmic scale. The error due to the error in rotation velocities is about ± 0.05. Hence, the effective error of SMD calculation is estimated to be ± 0.1–0.15.

In Figures 5 and 6 the SMD profiles of Sb and Sc galaxies are shown together. Although some Sc galaxies distinctly have smaller SMD values than the average, the difference in SMDs between the two galaxy types is fairly small. Namely, Sb and Sc galaxies show similar surface mass distributions. In the disk region at radii 3–10 kpc the SMD decreases exponentially outward by about 0.3 times per 5 kpc. In the bulge region (<2 kpc) of some galaxies, the SMD shows a power-law decrease, much steeper than an exponential decrease. This may indicate that the surface mass concentration in the central region is higher than the luminosity concentration. The central activities appear to be not directly correlated with the mass distribution. Note that the present sample includes galaxies showing Seyfert characteristics (NGC 1068, NGC 4569), LINERs (NGC 3521, NGC 4569), jets (NGC 3079), and black holes (the Milky Way).

3. LUMINOSITY PROFILES

3.1. *Data Selection*

Luminosity profiles in bulge regions are affected by the interstellar extinction. The extinction is higher nearer the center; it is higher for a larger inclination angle. It is also higher in shorter wave ranges. In fact, the color gradient ($B-K$ or $V-K$) between the bulge and disk for galaxies with larger inclinations ($i \geq 60°$) is greater than that for lower inclination galaxies (Héraudeau, Simien, & Mamon 1996). On the other hand, galaxies with $i \leq 51°$ in de Jong &

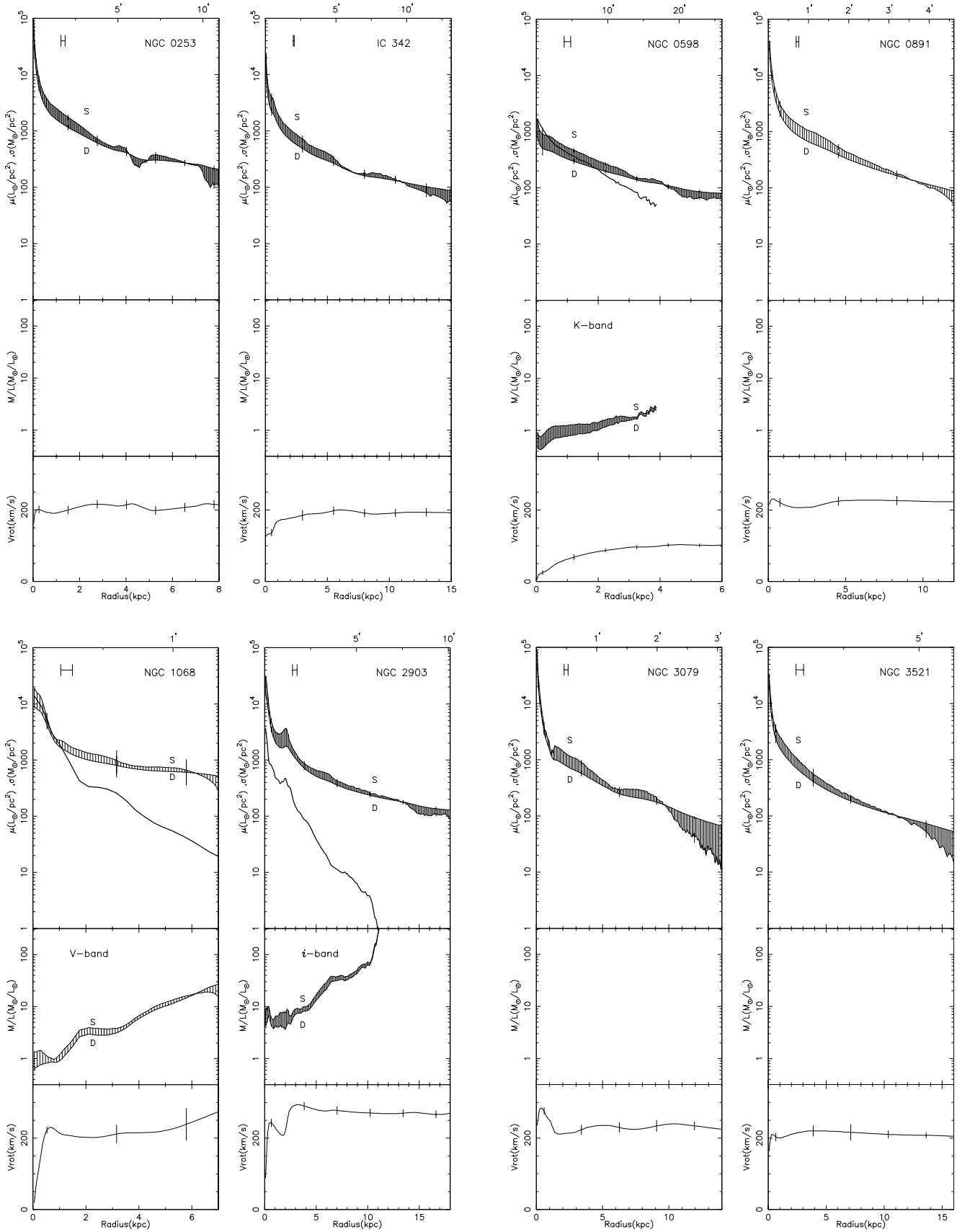

FIG. 4.—*Top panels*: Surface mass density profile for spherical (S) and flat-disk (D) assumptions. The luminosity profile (*heavy line*) corrected for the inclination is shown. *Middle panels:* Mass-to-luminosity ratios for spherical (S) and flat-disk (D) assumptions. *Bottom panels:* Rotation curve. The error bars are caused mainly by the errors of the rotation curve. The true values of the surface mass density will lie in the shaded area between S and D. The horizontal error bar (*upper left corner*) denotes the angular (spatial) resolution of the surface mass density (FWHM), which is larger than that of the luminosity profile in all the cases. The interval of the shading lines corresponds to double the interval of data sampling points.

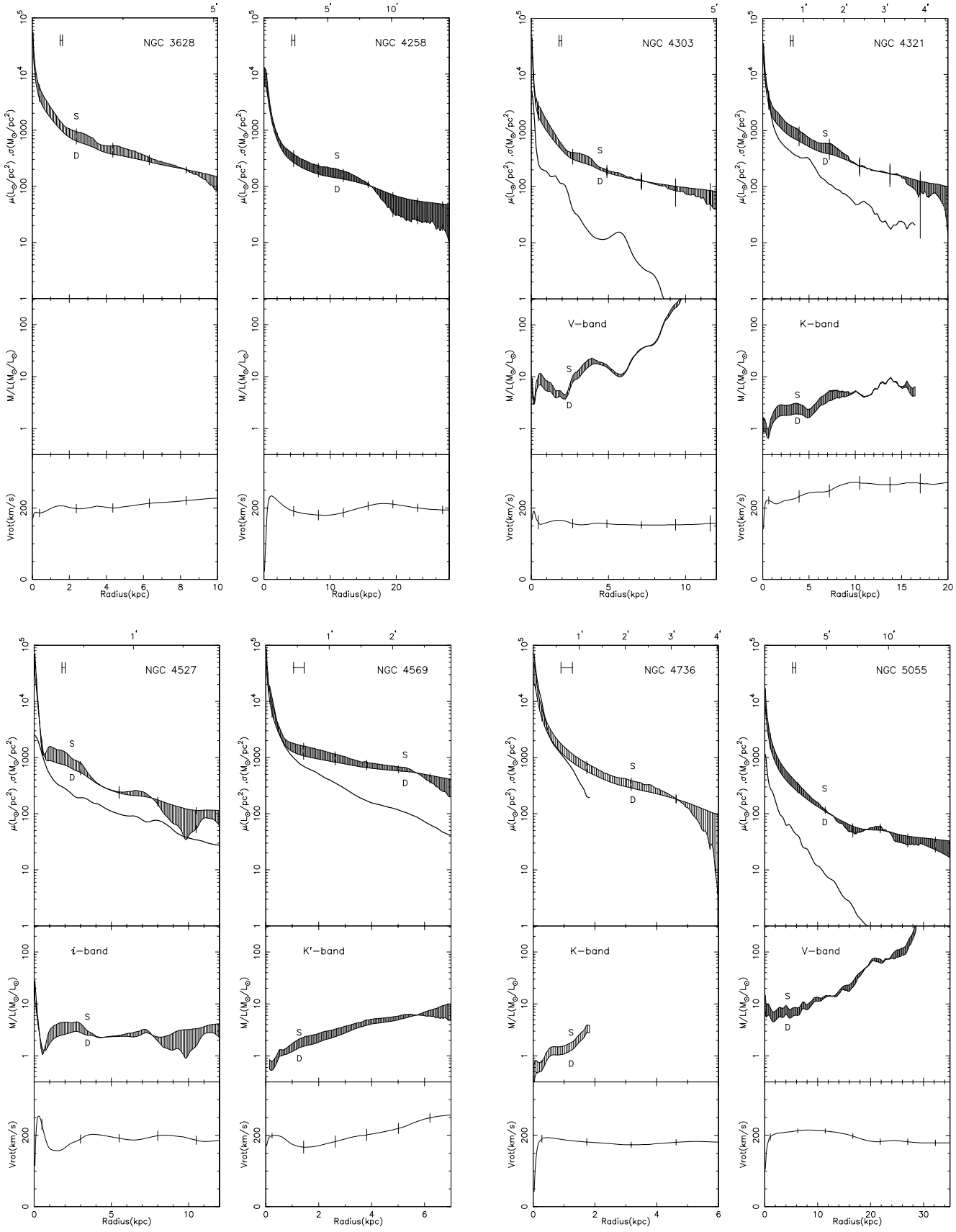

FIG. 4.—*Continued*

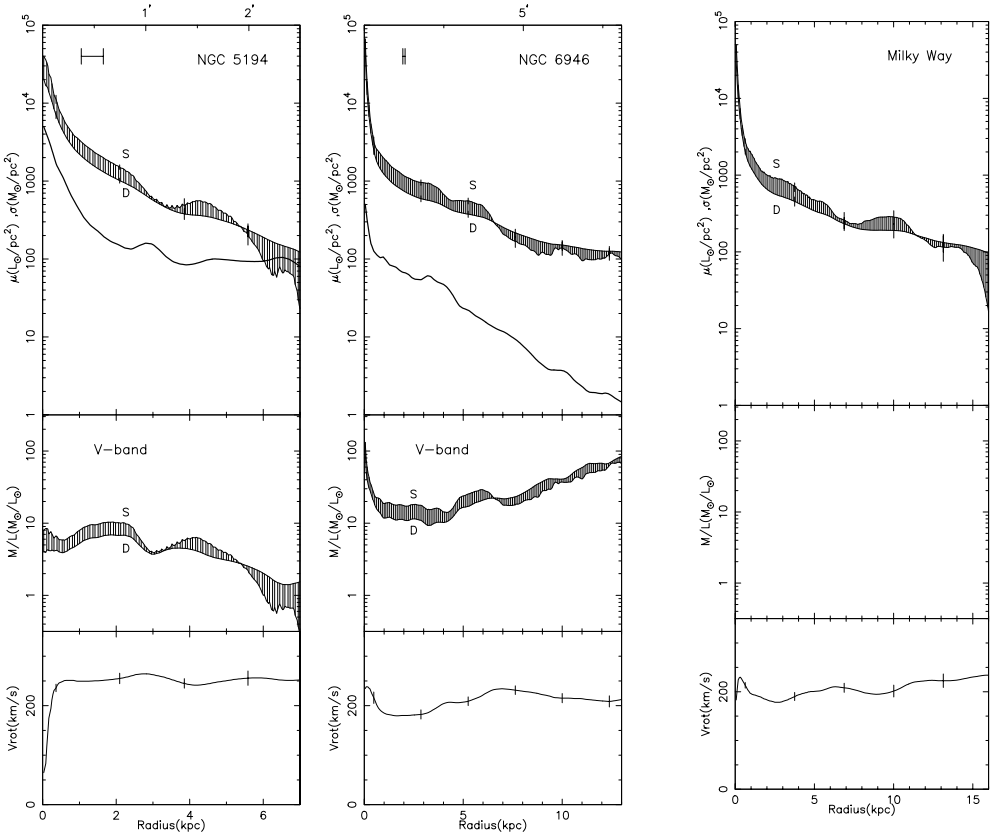

FIG. 4.—*Continued*

TABLE 1

PARAMETERS OF THE SAMPLE

				Rotation Curve Angular Resolution			Luminosity Profile	
Galaxy Name	Morphological Type	Inclination	Distance			Photometric Band	Angular Resolution	
(1)	(2)	(deg) (3)	(Mpc) (4)	(arcsec) (5)	(kpc) (6)	(7)	(arcsec) (8)	Reference (9)
NGC 253	Sc	78.5	2.5	15	0.18	…	…	…
IC 342	Sc	25	3.9	4	0.076	…	…	…
NGC 598 (M33)	Sc	54	0.79	55	0.21	*K*	2	(1)
NGC 891	Sb	88.3	8.9	4	0.17	…	…	…
NGC 1068 (M77)	Sb Sy	46	18.1	5 × 4	0.44 × 0.35	*V*	3	(2)
NGC 2903	Sc	35	6.1	15	0.44	*i*	1.2	(3)
NGC 3079	Sc	~90	15.6	4	0.30	…	…	…
NGC 3521	Sbc	75	8.9	15	0.65	…	…	…
NGC 3628	Sb	>86	6.7	3.9	0.13	…	…	…
NGC 4258 (M106)	Sbc	67	6.6	15	0.48	…	…	…
NGC 4303	Sc	27	8.1	4	0.16	*V*	3	(2)
NGC 4321 (M100)	Sc	27	15	4	0.29	*K*	1.8	(4)
NGC 4527	Sb	69	22	2.0	0.21	*i*	1.2	(3)
NGC 4569 (M90)	Sab	63	8.2	9.9 × 4.8	0.39 × 0.19	*K′*	2	(5)
NGC 4736 (M94)	Sab	35	5.1	15	0.37	*K*	1	(6)
NGC 5055 (M63)	Sbc	55	8	15	0.58	*V*	4	(2)
NGC 5194 (M51)	Sc	20	9.6	13	0.60	*V*	4	(2)
NGC 6946	Sc	30	5.5	4	0.11	*V*	3	(2)
Milky Way	Sb	90	0	…	…	…	…	…

NOTE.—Cols. (5), (6), and (8) are shown as FWHM.

REFERENCES.—Except for NGC 4527, Cols. (2)–(6) are taken or calculated from Sofue (1997), while for NGC 4527 they are from Sofue et al. (1998). Cols. (7) and (8) are taken from their references. For the luminosity profile: (1) Regan & Vogel (1994); (2) Kodaira et al. (1990); (3) Frei et al. (1996); (4) de Jong & van der Kruit (1994); (5) Boselli et al. (1997); (6) Möllenhoff et al. (1995).

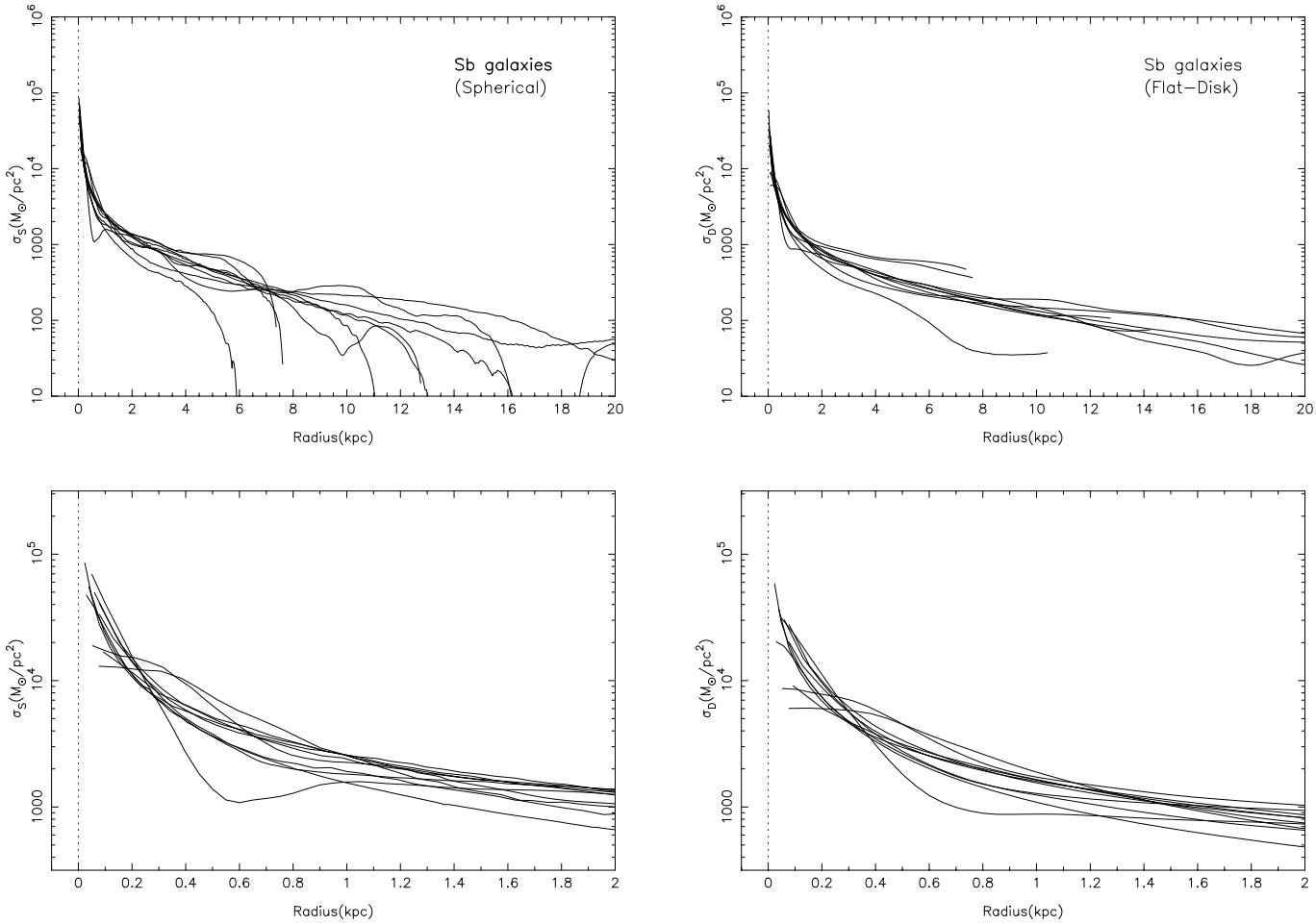

FIG. 5.—*Top Left:* Surface mass density profiles of Sb galaxies calculated for the spherical assumption. Because of the edge effect of the integration of eq. (3), the SMD curves decline rapidly in the outer 2–3 kpc region, where we must not rely on the obtained SMD profiles. *Bottom Left:* Same but for the inner region at $r = 0$–2 kpc. *Right:* Same as left panels but for the flat-disk assumption.

van der Kruit (1994) do not show significant differences in the color gradient.

In the present analysis, we have selected the galaxies whose inclinations are less than 70° if they are observed in the NIR and *i* bands and the galaxies with inclinations less than 60° if their data are in optical. In the latter case their mean surface luminosities may be weakened by 1 mag arcsec^{-2} at most, depending on the inclination. We have, thus, selected 11 galaxies from the 19 RC-selected galaxies.

3.2. *Description of the Data*

Table 1 lists the parameters for individual galaxies and their references. Since the data have been reduced in different ways by different authors, we have checked whether their data are suitable for the present analysis of M/L. We briefly describe the data, particularly how the surface luminosity profiles, $\mu(r)$, have been obtained.

1. Regan & Vogel (1994) deprojected NGC 598 and calculated $\mu(r)$ mag arcsec^{-2} by averaging azimuthally in rings of width $\pm 3''$. The deviation from axisymmetry is at most about 0.1 mag arcsec^{-2} including the observational error, which is much smaller than the error of the SMD. The effects caused by spiral arms are small.

2. and 3. Kodaira, Okamura, & Ichikawa (2; 1990) and de Jong & van der Kruit (3; 1994) measured $\mu(r)$ along the major axes. The errors of $\mu(r)$ are as small as $\sim \pm 0.1$–0.15 mag arcsec^{-2}.

4. Frei et al. (1996) published imaging data of spiral galaxies in Flexible Image Transport System (FITS) format. We have used them to derive $\mu(r)$ at the same position angles at which the RCs have been measured. The errors of $\mu(r)$ are found to be smaller than that of the SMD.

5. Boselli et al. (1997) reduced their data in the same way as Regan & Vogel (1994) to derive luminosity profiles. For NGC 4569 they assumed an inclination of 67° and a position angle of 23°, which are almost the same as those we adopt here. The errors of $\mu(r)$ are less than 0.1 mag arcsec^{-2} between $r = 0''$ and $150''$.

6. Möllenhoff, Matthias, & Gerhard (1995) calculated $\mu(r)$ of NGC 4736 along the semimajor axis for different position angles and ellipticities. Because of the central weak bar, $\mu(r)$ may be about 0.5 mag arcsec^{-2} brighter at $r = (10 \pm 5)''$ than that at the position angle of 108° as adopted for the RC.

We thus consider the errors in the luminosity profiles caused by the different methods to be negligible compared to those due to the observations, except for NGC 4736. We note, however, that observations in the *V* band (NGC 4303, NGC 5055, and NGC 6946) may be affected by spiral arms, and the errors will amount to about ± 0.5 mag arcsec^{-2} [$\sim \pm 0.2$ in units of log ($L_\odot$ pc^{-2})].

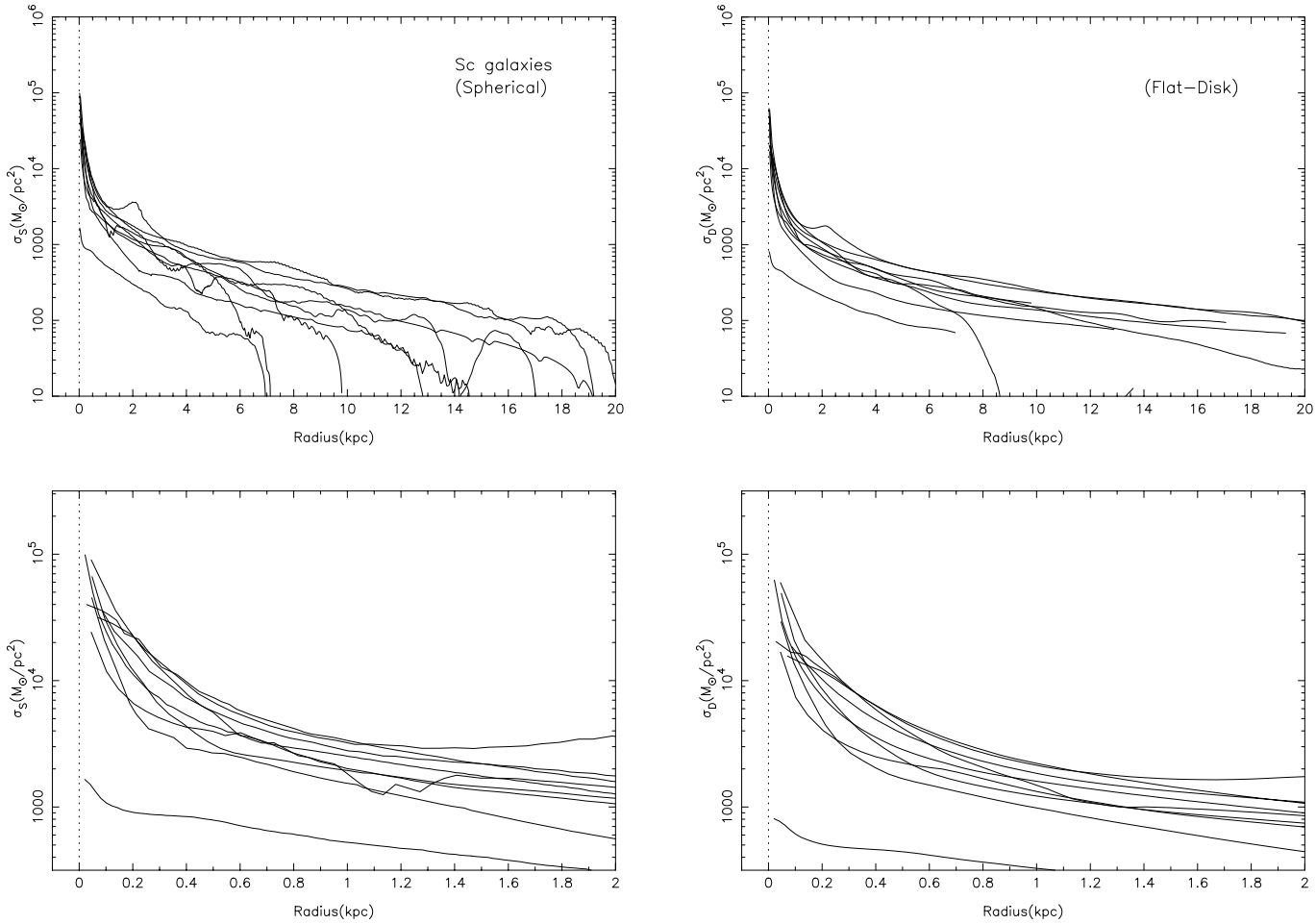

FIG. 6.—Same as Fig. 5, *left panels*, but for Sc galaxies. Note that some Sc galaxies show smaller SMD values than the total average of our sample. The Scd galaxy NGC 598 shows the smallest values in $r = 0$–6 kpc. The peculiar behavior of NGC 5194 at $r \sim 8$ kpc may be due to tidal interaction with its companion. *Right:* Same as left panels but for the flat-disk assumption.

4. MASS-TO-LUMINOSITY RATIOS

To obtain M/L profiles, we first converted the unit of $\mu(r)$ from mag arcsec^{-2} to $L_\odot$ pc^{-2}, then divided the SMD by $\mu(r)(L_\odot$ pc$^{-2}) \times \cos i$ corrected for the inclination. We adopt the following solar luminosities in the individual bands: $L_{\odot,V} = 4.83$, $L_{\odot,K} = 3.41$, $L_{\odot,K'} = 3.45$, and $L_{\odot,i} = 4.83$ mag. We note, however, that we cannot compare the absolute values of M/L profiles directly among the galaxies, because we use different filters for different galaxies. Hence, we here focus on relative variations of M/L with radius in each individual galaxy rather than comparing the absolute M/L values among different objects. Figure 4 shows the thus obtained M/L profiles for the 11 galaxies, and Figure 7 shows the same but for the inner 4 kpc region. As the errors of SMD are much larger than those of $\mu(r)$ for all the galaxies, only the errors in SMD are indicated.

4.1. *Results for Individual Galaxies*

We discuss the results for the individual galaxies as follows.

NGC 598.—This is a small-mass galaxy that has a mildly rising RC reaching only about 100 km s^{-1} in the disk region. The M/L increases slowly by 1.7 times from $r = 1$ to 3 kpc. In the bulge region it appears to decrease inward rapidly, with large errors. It also appears to increase inward within 150 pc, but that is not conclusive because the spatial resolution is 210 pc.

NGC 1068.—The M/L in the disk region increases slowly by 4.6 times from $r = 2$ to 6 kpc. In the bulge region it decreases more rapidly (0.28 times from $r = 2$ kpc to 800 pc) than in the disk but within $r = 800$ pc turns to be nearly flat or somewhat increasing. This is a type 2 Seyfert galaxy, so the luminosity profile in the V band may be not exact in the central region.

NGC 2903.—Both the SMD profile and $\mu(r)$ have a remarkable bump at $r \sim 2$ kpc. Since the shape of the RC is also peculiar, we may not neglect the effect of a non-axisymmetric component such as caused by a spiral arm. Interestingly, however, there appears no corresponding bump in the M/L. The M/L in the disk region increases slowly by 5.5 times from $r = 4$ to 9 kpc. This Sc galaxy has a compact bulge, and we cannot evaluate the M/L of the inner bulge because of the insufficient spatial resolution.

NGC 4303.—Because of some irregularities caused by spiral arms, the M/L in the disk region behaves irregularly, although it increases outward on the average. In the compact bulge region the M/L decreases inward steeply from $r = 2$ kpc to 500 pc. It then turns to increase within $r = 200$ pc toward the center.

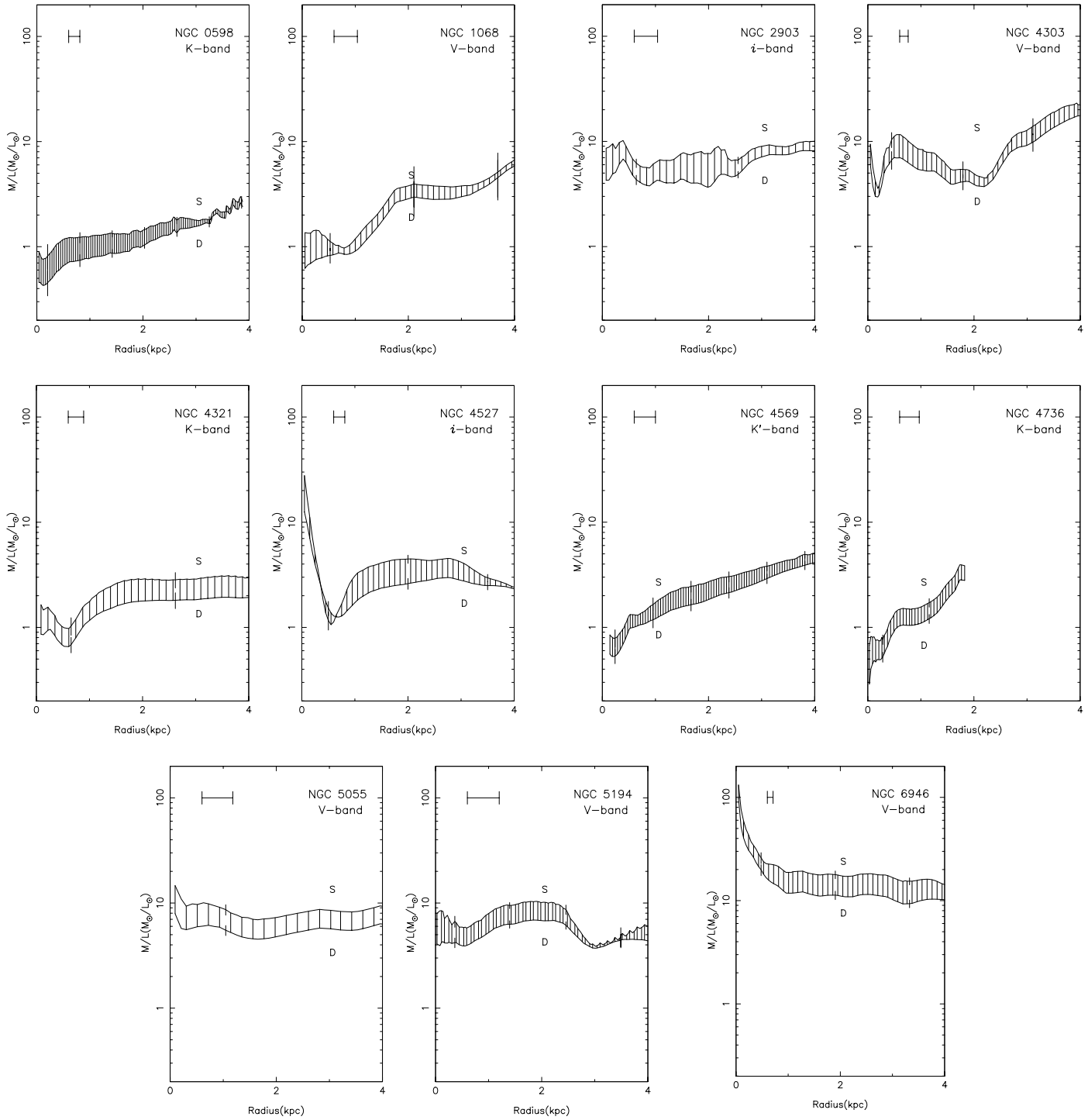

FIG. 7.—M/L profiles at $r = 0$–4 kpc for (S) the spherical assumption and (D) the flat-disk assumption. The meanings of the horizontal and vertical error bars and the shaded area are same as those in Fig. 4.

NGC 4321.—The M/L in the disk increases slowly by 2.0 times from $r = 3$ to 8 kpc. In the bulge region it seems to decrease inward and then increase near the center, though the error is large. Some luminous bumps of about 0.5 mag arcsec^{-2} are found at $r = 700$ pc and 5 and 11 kpc, which may be caused by spiral arms. The M/L increases systematically inward by about 2 times from $r = 300$ to 150 pc.

NGC 4527.—The M/L in the disk region is almost flat or slowly increases outward. In the bulge region it decreases inward from $r = 2$ kpc to 500 pc. Then it turns to increase steeply toward the center.

NGC 4569.—The M/L in the disk region increases by 2.4 times from $r = 2$ to 5 kpc. In the bulge region it appears to decrease inward and then turns to increase toward the center. However, the spatial resolution is not sufficient to confirm the central increase.

NGC 4736.—The luminosity profile is obtained only in the bulge region. The M/L in the bulge region decreases

distinctly inward by 0.38 times from $r = 1.8$ kpc to 800 pc. The M/L in the innermost region cannot be evaluated because of the large spatial resolution.

NGC 5055.—The M/L in the disk region increases slowly by 3.0 times from $r = 5$ to 15 kpc. In the bulge region its variation is difficult to evaluate because of the insufficient resolution as well as because of the large error in the luminosity profile caused by spiral arms. It looks flat in the outer bulge and increases inward in the inner bulge region.

NGC 5194.—The M/L in the disk region is almost flat or rather decreases outward. The peculiar behavior of the SMD, and therefore of the M/L, is probably due to an RC disturbed by tidal interaction with the companion galaxy NGC 5195. In the bulge region, the M/L is flat or slightly decreases inward to $r = 700$ pc. Within $r = 700$ pc, it looks flat or slightly increasing, while the spatial resolution is not sufficient to reveal the details.

NGC 6946.—The SMD profile for this galaxy has been calculated with the highest accuracy among the 11 galaxies of the present sample (FWHM of 110 pc). The M/L in the disk region is flat from $r = 1$ to 3 kpc, and then it increases slowly by 2.8 times from $r = 3$ to 10 kpc. In the compact bulge region, it shows a remarkable increase toward the center by about an order of magnitude from $r = 1$ kpc to 50 pc.

4.2. *General Characteristics*

From Figures 4 and 7 we summarize the general characteristics of the M/L behavior as follows.

1. The M/L remains nearly constant in the inner disk.
2. It increases gradually outward in the outer disk for all the galaxies, except for NGC 5194, which is tidally disturbed by its companion.
3. The M/L increases more steeply in the outer halo, indicating the massive dark halo.
4. Bulge components show a constant or a slightly smaller value than the disk value.
5. For NGC 4527 and NGC 6946 the M/L increases steeply toward the nucleus inside the bulge.

This drastic increase in M/L within $r = 500$ pc for NGC 4527 and NGC 6946 is of particular interest: for NGC 4527 this increase amounts to 4.9 ± 1.0 times per 350 pc from $r = 500$ to 150 pc, and for NGC 6946, 3.5 ± 0.9 times per 500 pc from $r = 600$ to 100 pc. Since the results are based on optical data, these values may be overestimated because of optical extinction. However, it is known that color gradients such as $V-K$ and $R-K$ of face-on galaxies are of the order of 1 mag arcsec^{-2} (e.g., de Jong & van der Kruit 1994; Terndrup et al. 1994). Therefore, we may conclude that the increase in M/L for NGC 6946, whose inclination is only 30°, is significantly greater than that expected from the optical extinction effect. For NGC 4527 with $i = 60° \sim 75°$, the $B-K'$ color gradient is estimated to be about 1.5 mag arcsec^{-2} (Héraudeau et al. 1996). In the present data, the luminosity profile of NGC 4527 is in the Thuan-Gunn i band, and we may conclude that the central increase of M/L for NGC 4527 will be also significant.

Such a remarkable increase in M/L toward the center is, however, not detected in the other galaxies. For NGC 1068, NGC 2903, NGC 4303, NGC 4569, NGC 4736, and NGC 5194, the spatial resolution is not sufficient to reveal such an increase even if it did exist. For NGC 4321 and NGC 5055 we see some hints of a possible central increase. For the small-mass galaxy, NGC 598, we cannot find any increase inward near the center.

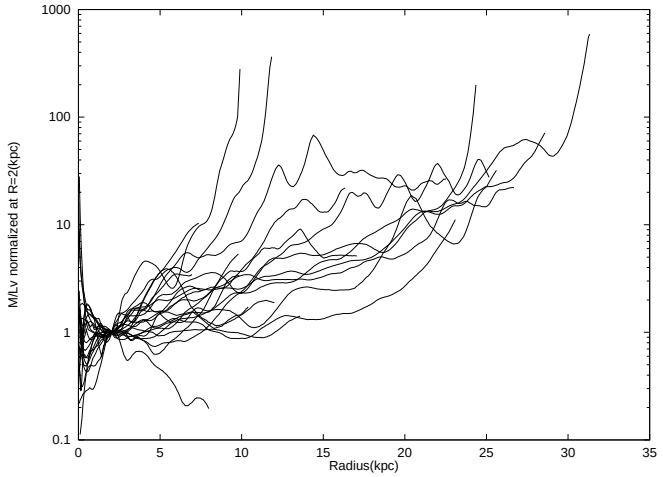

FIG. 8.—M/L distributions normalized at $r = 2$ kpc, as obtained by using the SMD and the V-band photometric data of Kodaira et al. (1990).

In current studies of the M/Ls of spiral galaxies, the bulge and disk M/Ls have been assumed to be radially constant. However, this does not necessarily mean that the total M/L value is constant in the region corresponding to each component: in Figure 8 we present the variations in the M/L for galaxies with inclinations less than 80°. Here, the M/L value is normalized to unity at $r = 2$ kpc. It is now obvious that the total M/L is not constant at all within a galaxy but varies significantly in the bulge and disk, not only in the massive halo. The M/L value often increases outward by 100 times per $\sim$10–30 kpc from the disk to the outer halo. The only exception is NGC 5194, whose peculiar M/L behavior is due to tidal interaction with the companion.

5. DISCUSSION

5.1. *Massive Dark Core*

We have used high-accuracy RC data to derive SMD profiles for 19 galaxies and M/L profiles for 11 galaxies. For three galaxies, NGC 598, NGC 4527, and NGC 6946, we obtained both high spatial resolution ($r \leq 200$ pc) RCs and luminosity profiles without large irregularities due to spiral arms and/or bars. Among these three galaxies, two galaxies, NGC 4527 and NGC 6946, are found to show a steep inward increase of M/L in the central region, $r \leq 500$ pc. Such a steep central increase of M/L may imply that the bulges contain an excess of dark mass inside a few hundred pc, which we call a "massive dark core" with a scale radius of $\sim$100–200 pc. This yields a mass of $M \sim RV^2/G \sim 10^9$ $M_\odot$, assuming $V(R = 100\text{–}200 \text{ pc}) = 200$ km s^{-1}. The massive dark cores could be objects linking the galactic bulges with massive black holes in the nuclei (Miyoshi et al. 1995; Genzel et al. 1997; Ghez et al. 1998) and/or massive core objects causing a central Keplerian RC (Bertola et al. 1998).

For the Sbc galaxy NGC 4527 we have detected both a dark core and a normal bulge within the luminous bulge region. For the Scd galaxy NGC 6946 we found the dark core, whereas we could hardly detect a normal bulge component. On the other hand, we could see only a normal bulge component in the Scd galaxy NGC 598. Such a difference may indicate that the existence of a dark core may not be directly related to the morphology. It is also interesting to note that the scale sizes of the dark cores in the two

galaxies may not be uniquely correlated to the sizes of luminous bulges. Although dark cores will have a crucial implication for the formation, evolution, and dynamics of the central bulges of galaxies, their origin and universal properties remain open to discussion.

5.2. *Dark Mass Fraction*

It is interesting to derive the distribution of the dark mass fraction (DMF), $F_{\rm DM}$, defined by the local dark-to-total mass density ratio at a given r. If the luminosity profile can be corrected for the extinction, we can define the following quantity:

$$\frac{\sigma_{\rm total}}{\mu_*}(r) = \frac{\sigma_* + \sigma_{\rm dark}}{\mu_*}, \tag{6}$$

where $\sigma_{\rm total}$, σ_*, $\sigma_{\rm dark}$, and μ_* denote the SMD of the total mass, visible mass, dark mass, and the surface luminosity density, respectively. If the M/Ls of stars on the average at a given r, which will be derived from luminosity profiles by multiband observations in optical and infrared bands, is known, then we can define the DMF by

$$F_{\rm DM}(r) = \frac{\sigma_{\rm dark}}{\sigma_{\rm total}} = \frac{\sigma_{\rm total}/\mu_*(r) - \sigma_*/\mu_*(r)}{\sigma_{\rm total}/\mu_*(r)}. \tag{7}$$

This quantity can be used to evaluate the dark matter distribution.

Since the absolute calibration of the stellar M/Ls and the precise correction for the extinction are beyond our scope, here we only briefly attempt to examine qualitative trends of variation of the DMF. We examine the following two cases. In one case, we assume $\sigma_*/\mu_*(r)$ to be constant and equal to $\sigma_{\rm total}/\mu_*(r)$ in the inner disk region; in the other case, we take it equal to one-half that. We thus derive $F_{\rm DM}(r)$ and $\sigma_{\rm dark}(r)$ for NGC 6946: the results are shown in Figure 9, left and right panels, corresponding to the above two cases, respectively. Since $\sigma_*/\mu_*(r)$ will be smaller in the outer disk region owing to the dominance of younger stars of lower metallicity (e.g., de Jong 1996), we may safely consider that the DMF is at least $\sim$80%–90% in the outer disk beyond 8 kpc. In the inner disk region ($r \sim 4$–5 kpc) the DMF appears to be more than 50%. However, the uncertainty is too large to give a more detailed discussion.

5.3. *Dark Mass versus Visible Mass in the Disk Region*

The radial distribution of DMF can be used to derive individual distributions of dark mass and visible mass in the disk region. We attempt the following analysis.

1. We fit the observed luminosity profiles on a logarithmic scale by a nonlinear least-squares fit by a model, which consists of an exponential bulge and an exponential disk. The model is given by

$$\mu_{\rm model}(r) = \mu_{\rm disk}(r) + \mu_{\rm bulge}(r), \tag{8}$$

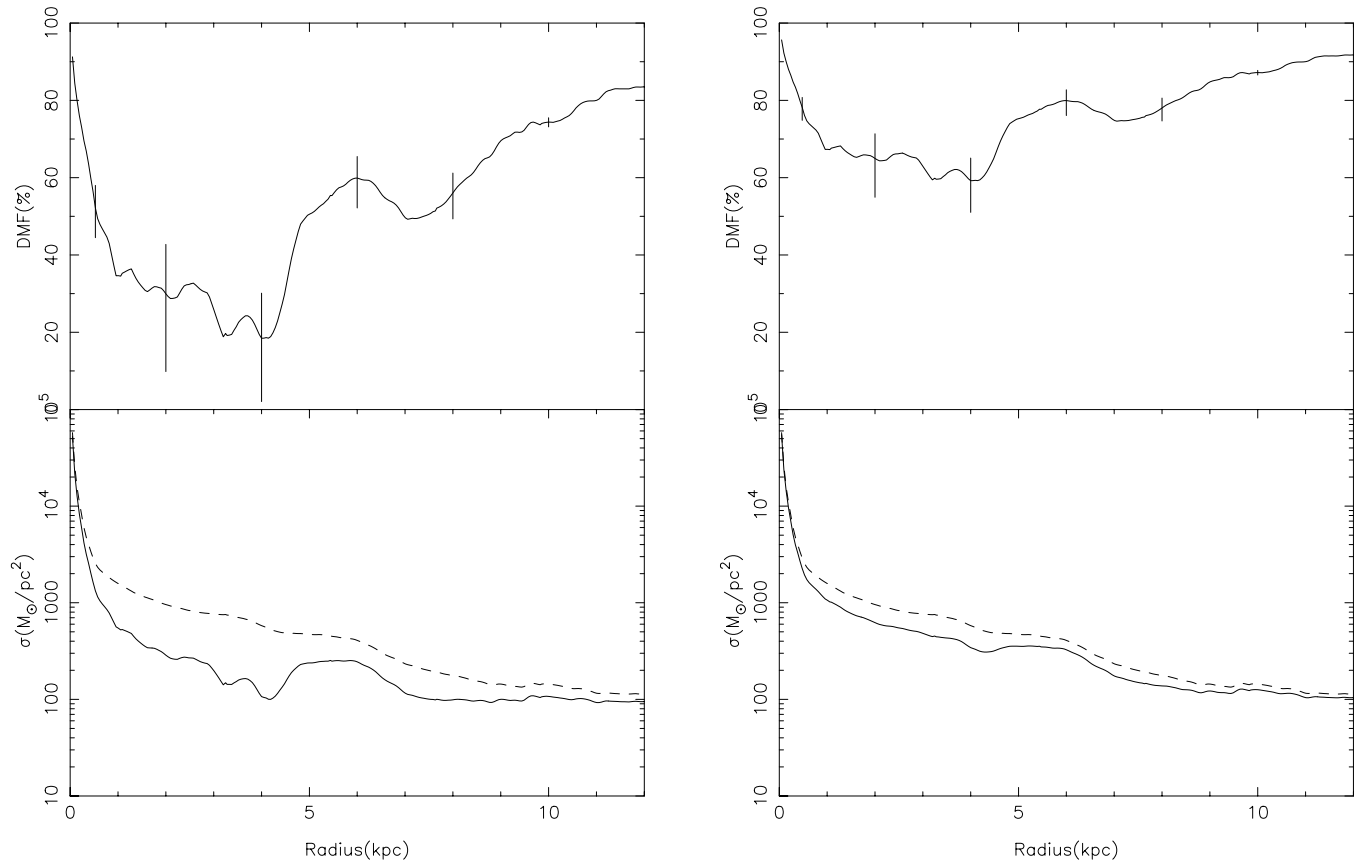

FIG. 9.—*Top Left:* Distribution of the DMF in NGC 6946 for a case of $\sigma_*/\mu_*(r) = 10$. The error bars are due to the difference between the assumptions of spherical and flat-disk mass distributions. Note that the DMF is more than 50% even in the disk region. *Bottom Left:* SMD distribution of the dark mass (*solid line*) and the total mass (*dashed line*). *Right:* Same as left panel but for $\sigma_*/\mu_*(r) = 5$. Note that more than half the total mass is dominated by dark mass in $r \geq 5$ kpc not strongly depending on $\sigma_*/\mu_*(r)$.

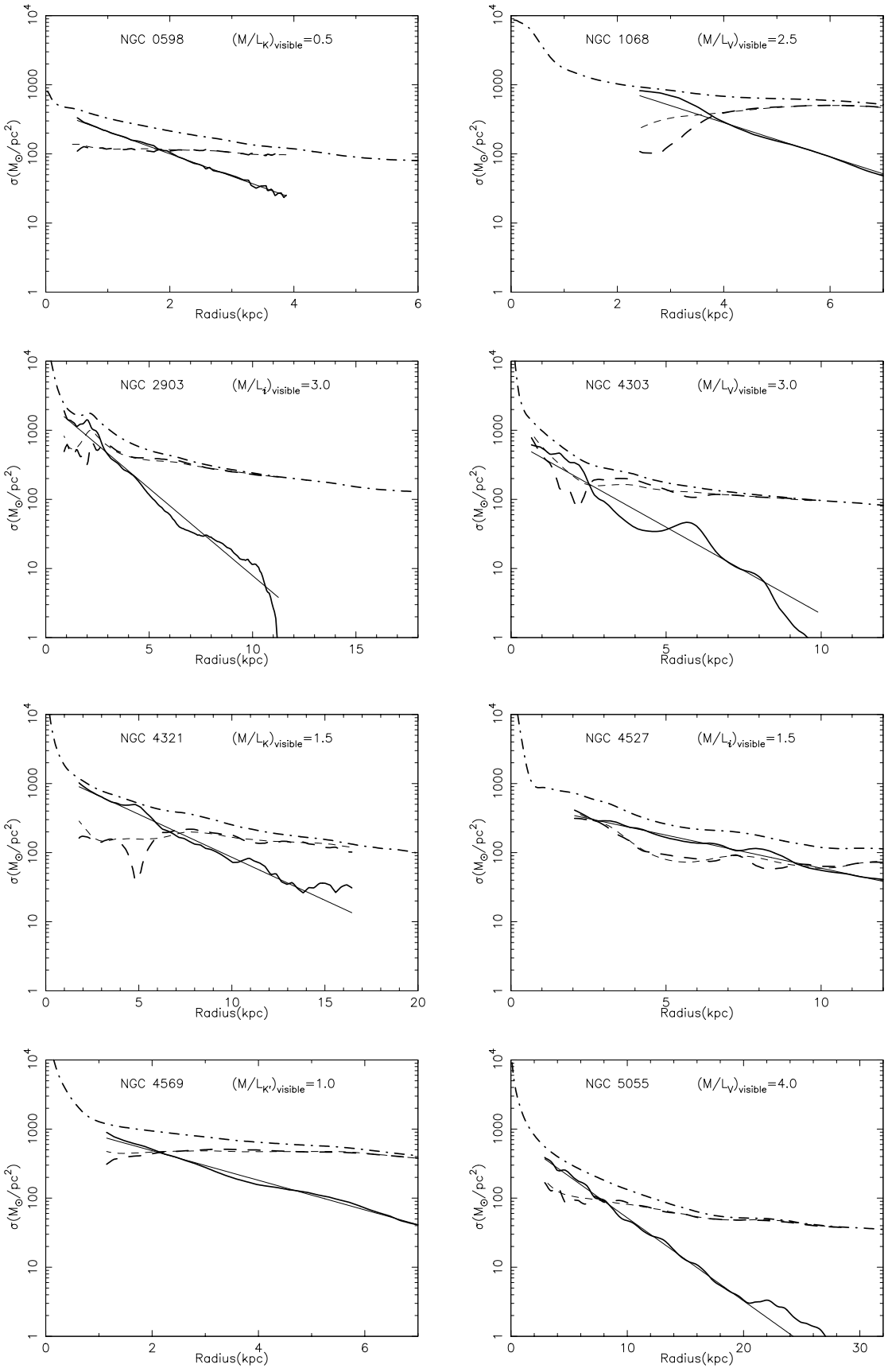

FIG. 10.—SMD profiles of the total mass (*dot-dashed lines*), visible mass (*solid lines*), and dark mass (*dashed lines*). The light lines are based on the two-component model, while heavy lines are directly calculated from the data.

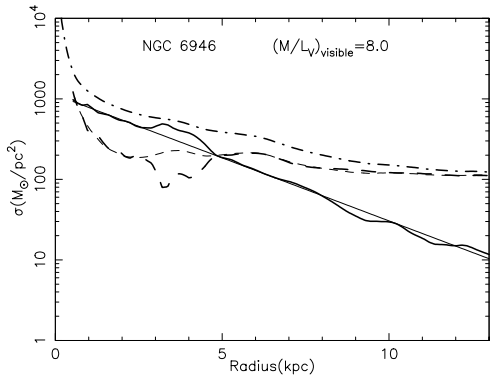

FIG. 10.—*Continued*

TABLE 2

THE FITTING PARAMETERS

Galaxy	$\mu_{e,\rm disk}$ ($L_\odot$ pc^{-2})	$r_{e,\rm disk}$ (kpc)	$\mu_{e,\rm bulge}$ ($L_\odot$pc^{-2})	$r_{e,\rm bulge}$ (kpc)	r_0 (kpc)	$r_{\rm mb,max}$ (kpc)	$(M/L)_{\rm visible}$ ($M/L_\odot$)
NGC 598.....	166.	2.25	205.	0.29	0.50	1.8	0.5
NGC 1068.....	205.	2.94	2926.	0.63	2.39	3.5	2.5
NGC 2903.....	164.	2.89	575.	0.35	0.85	2.0	3.0
NGC 4303.....	44.	2.90	1258.	0.18	0.65	2.6	3.0
NGC 4321.....	187.	5.86	3265.	0.53	1.79	7.2	1.5
NGC 4527.....	67.	7.62	552.	0.70	2.03	10.1	1.5
NGC 4569.....	243.	3.41	6530.	0.31	1.13	2.1	1.0
NGC 5055.....	39.	6.06	196.	1.00	2.83	8.0	4.0
NGC 6946.....	26.	4.65	96.	0.21	0.48	4.7	8.0

where

$$\mu_{\rm disk}(r) = \mu_{e,\rm disk}\, e^{-1.679(r/r_{e,\rm disk}-1)} \tag{9}$$

and

$$\mu_{\rm bulge}(r) = \mu_{e,\rm bulge}\, e^{-1.679(r/r_{e,\rm bulge}-1)}\,. \tag{10}$$

We successfully fitted the data using this model for nine galaxies, except for NGC 4736 and NGC 5194: NGC 4736 was short of the data in the disk region, and NGC 5194 does not have a disk described by the exponential function probably because of the tidal interaction.

2. We define boundary radius, r_0, at which $\mu_{\rm disk}/\mu_{\rm bulge} = 10$, and assume that the M/L of visible mass, σ_*/μ_*, is constant outside of r_0. We will focus on the disk region in the following.

3. We set the M/L value at $r = r_0$ to that of the total mass, so that the visible mass becomes maximum in each galaxy. From the consideration in § 2.3, we adopt a flat-disk mass distribution for SMDs. By subtracting the SMDs of visible mass from those of total mass, we obtain distributions of dark mass for the nine galaxies. We define the "mass boundary radius," $r_{\rm mb}$, outside of which the fitted SMDs of visible mass are dominated by the dark mass. Note that, because of the assumption of maximum M/L of visible mass, we in fact derive the maximum mass boundary radius, $r_{\rm mb,max}$, inside of which dark mass may even exceed visible mass.

In Figure 10, we show the results of SMD profiles of the total, visible, and dark mass for each galaxy. The parameters are listed in Table 2. Two interesting points are found: first, dark mass tends to dominate visible mass even in the inner disk region. In Figure 11, the relation between the

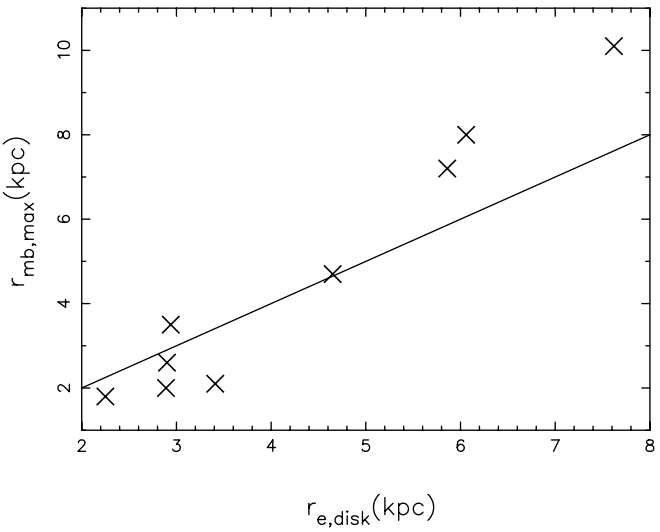

FIG. 11.—Relation between $r_{e,\rm disk}$ and $r_{\rm mb,max}$. The straight line shows $r_{\rm mb,max} = r_{e,\rm disk}$.

effective radius of a disk component, $r_{e,\mathrm{disk}}$, and $r_{\mathrm{mb,max}}$ is shown. As $r_{\mathrm{mb,max}}$ is an upper limit of r_{mb}, $r_{e,\mathrm{disk}}$ is approximately equal to or less than $r_{\mathrm{mb,max}}$. This trend appears to be independent of morphology, partly because the sample is biased to the late-type galaxy. Second, there may be a linear correlation between the two parameters in Figure 11. This trend is caused by the maximum M/L of visible mass in a disk. However, the M/Ls adopted here range from 0.5 to 4.0 except for NGC 6946, and even if the M/L values are halved, $r_{\mathrm{mb,max}}$ will be reduced by only a few kpc. This correlation may indicate that, if any, dark mass traces visible mass only up to $r = r_{e,\mathrm{disk}}$ at most and that the luminous scale of galaxies is almost independent of the distribution of a dark halo because the difference in SMD profiles is small (see Figs. 5 and 6).

REFERENCES

Athanassoula, A., Bosma, A., & Papaioannou, S. 1987, A&AS, 179, 23
Bertola, F., Cappellari, M., Funes, J. G., Corsini, E. M., Pizzella, A., & Vega-Bertran, J. C. 1998, ApJ, 509, L93
Binney, J., & Tremaine, S. 1987, Galactic Dynamics (Princeton: Princeton Univ. Press)
Boselli, A., Tuffs, R. J., Gavazzi, G., Hippelein, H., & Pierini, D. 1997, A&AS, 121, 507
Bosma, A. 1981a, AJ, 86, 1791
———. 1981b, AJ, 86, 1825
———. 1998, preprint (astro-ph/9812013)
Clemens, D. P. 1985, ApJ, 295, 422
de Jong, R. S. 1996, A&A, 313, 377
de Jong, R. S., & van der Kruit, P. C. 1994, A&AS, 106, 451
Forbes, D. A. 1992, A&AS, 92, 583
Frei, Z., Guhathakurta, P., Gunn, J., & Tyson, J. A. 1996, AJ, 111, 174
Genzel, R., Eckart, A., Ott, T., & Eisenhauer, F. 1997, MNRAS, 291, 219
Ghez, A. M., Klein, B. L., Morris, M., & Becklin, E. E. 1998, ApJ, 509, 678
Héraudeau, Ph., & Simien, F. 1997, A&A, 326, 897
Héraudeau, Ph., Simien, F., & Mamon, G. A. 1996, A&AS, 117, 417
Honma, M., & Sofue, Y. 1997a, PASJ, 49, 453
———. 1997b, PASJ, 49, 539
Kent, S. M. 1986, AJ, 91, 1301
———. 1987, AJ, 93, 816
Kodaira, K., Okamura, S., & Ichikawa, S. 1990, Photometric Atlas of Northern Bright Galaxies (Tokyo: Univ. Tokyo Press)
Mathewson, D. S., & Ford, V. L. 1996, ApJS, 107, 97
Mathewson, D. S., Ford, V. L., & Buchhorn, M. 1992, ApJS, 81, 413
Miyamoto, M., & Nagai, R. 1975, PASJ, 27, 533
Miyoshi, M., Moran, J., Herrnstein, J., Greenhill, L., Nakai, N., Diamond, P., & Inoue, M. 1995, Nature, 373, 127
Möllenhoff, C., Matthias, M., & Gerhard, O. E. 1995, A&A, 301, 359
Nordsieck, K. H. 1973, ApJ, 184, 719
Ostriker, J. P., & Peebles, P. J. E. 1973, ApJ, 186, 467
Persic, M., & Salucci, P. 1988, MNRAS, 234, 131
———. 1990, MNRAS, 245, 577
———. 1995, ApJS, 99, 501
Persic, M., Salucci, P., & Stel, F. 1996, MNRAS, 281, 27
Regan, M. W., & Vogel, S. N. 1994, ApJ, 434, 536
Rubin, V. C., Burstein, D., Ford, W. K., Jr., & Thonnard, N. 1985, ApJ, 289, 81
Rubin, V. C., Ford, W. K., Jr., & Thonnard, N. 1980, ApJ, 238, 471
———. 1982, ApJ, 261, 439
Rubin, V. C., Kenny, J. D. P., & Young, J. S. 1997, AJ, 113, 1250
Salucci, P., & Frenk, C. S. 1989, MNRAS, 237, 247
Shu, F. H., Stachnik, R. V., & Yost, J. C. 1971, ApJ, 166, 465
Sofue, Y. 1996, ApJ, 458, 120
———. 1997, PASJ, 49, 17
Sofue, Y., Tomita, A., Honma, M., Tutui, Y., & Takeda, Y. 1998, PASJ, 50, 427
Sofue, Y., Tutui, Y., Honma, M., & Tomita, A. 1997, AJ, 114, 2428
Sofue, Y., Tutui, Y., Honma, M., Tomita, A., Takamiya, T., Koda, J., & Takeda, Y. 1999, ApJ, 523, 136
Terndrup, D. M., Davies, R. L., Frogel, J. A., DePoy, D. L., & Wells, L. A. 1994, ApJ, 432, 518